

A support to the lattice compatibility theory: nanoscale patterns of manganese-doped lattices in terms of the Urbach energy and Faraday effect

Karemt Boubaker

École Supérieure de Sciences et Techniques de Tunis (ESSTT), Université de Tunis, 5100 Mahdia, Tunisia.
Fax: +216 73 68 1313; e-mail: mmbb11112000@yahoo.fr

DOI: 10.1016/j.mencom.2013.05.014

The manganese-doped crystals of bismuth titanates, germanates and sillenites are discussed in terms of the Urbach tailing and Faraday effect along with doping agent intrinsic lattice patterns.

Bismuth titanates, germanates and sillenites are well-known photorefractive materials used in surface acoustic wave devices, non-linear integral optics, laser resonators and phase-conjugated spatial-time light modulators. Doping agents induced lattice-scale and topological instability along with atomic-scale dispersion in these compounds.^{1–10} In the case of manganese doping, the ternary oxides Bi₁₂SiO₂₀ (BSO), Bi₄Ge₃O₁₂ (BGO) and Bi₄Ti₃O₁₂ (BTO) interact differently with manganese despite their chemical similarities.^{7–10}

Here, new elements of these differences are explained and discussed in the framework of the lattice compatibility theory (LCT).[†]

The chemical properties of Mn²⁺ ion are very similar to those of Zn²⁺. Wardzynski *et al.*¹⁵ used paramagnetic resonance spectra and Mn–element energetic levels scheme to prove that bismuth oxide crystals incorporate Mn²⁺ (and Mn⁴⁺) ions as a consequence of electron transition toward the conduction band (Figure 1).

According to Chen *et al.*,¹⁶ equilibrium structure of Mn doping atoms in host structures occurs due to two possible scenarios depending on energetic and kinetic considerations. Mn atoms

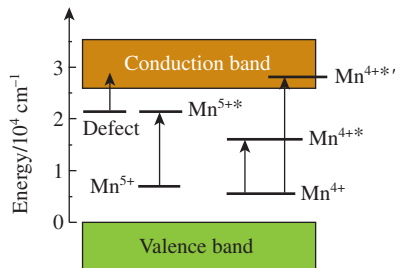


Figure 1 Mn-element energetic levels diagram.

[†] Bi₄Ti₃O₁₂ was prepared using a polymeric precursor method¹¹ from titanium tetra(isopropoxide) and bismuth acetate. Complexation and pH adjustment were achieved using wet ethylene glycol and ammonium hydroxide, respectively.

Bi₁₂SiO₂₀ and Bi₄Ge₃O₁₂ were grown from stoichiometric melts using the Czochralski method^{12–14} with high-purity Bi₂O₃, GeO₂ and SiO₂ as precursors. The Mn-doped samples were prepared by adding MnCO₃ and MnO₂ in various proportions. The concentrations of the doping agent in the crystals were determined using emission spectral analyses and chemical absorption with an accuracy of 6%.

X-ray diffraction analysis was performed on an Analytical X Pert PROMPD copper-source diffractometer ($\lambda = 1.54056 \text{ \AA}$), and the optical absorption spectra were measured on double-side polished parallel crystal plates using a SPM-2 monochromator to within $\pm 2 \text{ nm}$.

stabilize inside host matrices either in substitutional or interstitial positions. The energy cost for the transition from initial to final states during doping suggests interstitial positions inside Si matrices and substitutional positions inside Ti and Ge matrices.

In order to understand the Urbach tailing alteration following doping agent insertion into host structures, the Urbach energy E_u was determined for doped and undoped samples from the equations

$$\ln[\alpha(h\nu)] = \ln(\alpha_0) + \frac{h\nu}{E_u},$$

$$E_u = \alpha(h\nu) \left\{ \frac{d[\alpha(h\nu)]}{d[h\nu]} \right\}^{-1} = h \left\{ \frac{d}{d\nu} \ln[\alpha(\nu)] \right\}^{-1},$$

where $\alpha(h\nu)$ represents, for each sample, the experimentally deduced optical absorption profile.

The Urbach energy E_u is a measure of the inhomogenous instability and atomic scale dispersion inside structures as it indicates the width of the band tails of the localized states in the presence of defects (Figure 2). Its analytical formulation¹⁷ takes into account three components: structural disorder, carrier-phonon interaction and carrier impurity, respectively.

$$E_u = \frac{k_B U \theta_D}{2} + F \frac{4\pi^2 Z^2 q^4 m^* L_D^3}{9 \sqrt{3} \epsilon^2 \hbar^2} + F' \text{cth} \left(\frac{F''}{2k_B T} \right),$$

where k_B is the Boltzmann constant, U is the lattice strain related with the structural disorder, θ_D is the Debye temperature, L_D is the Debye length, m^* is the carrier effective mass, Z is the impurity charge, q is the electron charge, ϵ is the static dielectric permittivity, \hbar is the Planck constant, and F, F', F'' are constants.

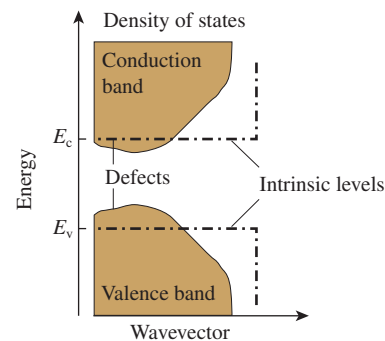


Figure 2 Urbach tailing and localized states in the presence of defects.

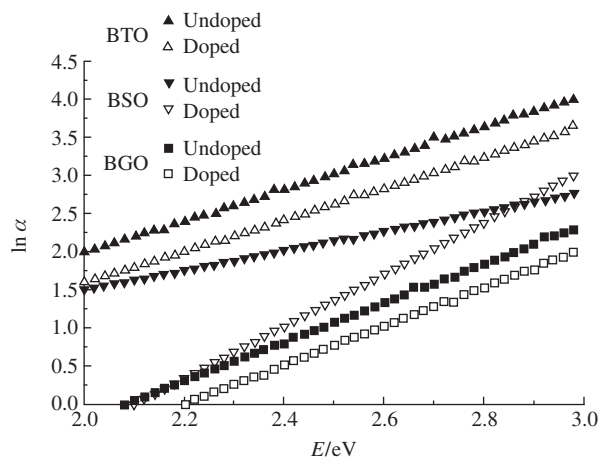


Figure 3 Plots of $\ln \alpha(\nu)$ vs. energy $h\nu$ (as guides for evaluating E_0).

The width of the localized states (band tail energy or Urbach energy E_0) was estimated from the slopes of the plots of $\ln \alpha(\nu)$ versus energy $h\nu$ (Figure 3).

The Faraday effect¹⁹ (or Faraday rotation effect) is a magneto-optical phenomenon that consists of an interaction between light and a magnetic field inside a medium. It causes a rotation of the plane of polarization, which is linearly proportional to the component of the magnetic field in the direction of propagation. The Faraday effect is based on the notion of circular birefringence, which causes a difference of propagation speed between left and right circularly polarized waves.

The Faraday effect for the test samples was evaluated by the measurements of alterations in the Verdet coefficient V within the visible spectral domain (Figure 4). This coefficient¹⁹ is deduced via the measurement of the polarisation rotating angle θ using the formula:

$$V = \frac{1}{Bl} \theta,$$

where B is the applied magnetic field strength (in oersteds), and l is the light path length through the medium.

Thus, the stability of Mn ions within a host matrix was different inside the three test lattice structures. The LCCT^{20–24} tries to give a plausible understanding of this disparity starting from intrinsic doping-element lattice properties in comparison to those of the host. In the test materials, changes in the Urbach energy and Faraday effect were due to a Mn-doping induced disorder in BSO matrices against a relative unaltered stability of both BGO and BTO. In this context, fundamental geometrical observations concerning the structure of BSO and the doping lattice are interpreted in terms of a comparison to manganese intrinsic lattice parameter (Figure 5).

As a first step, the main lattice constants of a Mn intrinsic lattice were compared to those of BSO, BGO and BTO. The fundamental geometrical observations concerning the structures

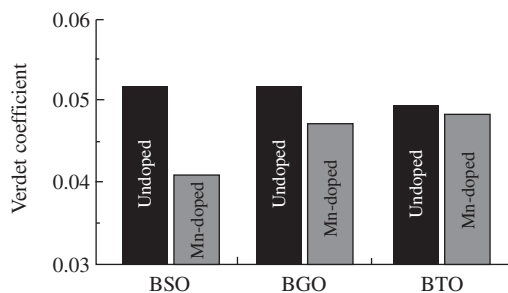


Figure 4 Verdet coefficient V changes for doped and undoped samples.

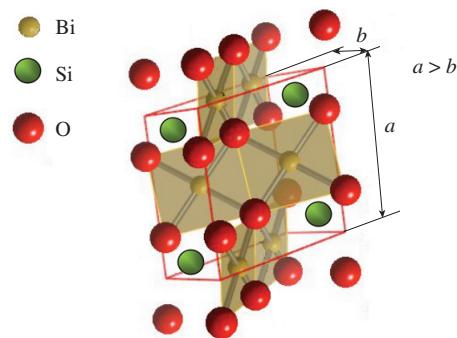


Figure 5 BSO lattice.

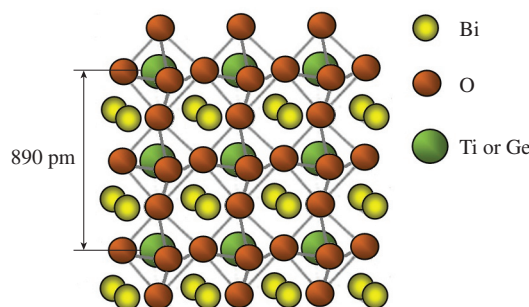


Figure 6 BTO and BGO lattices.

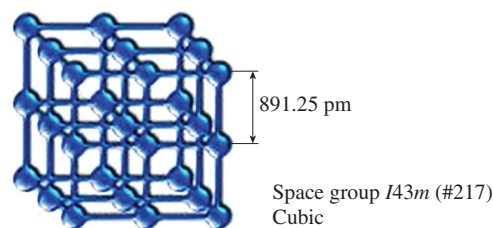


Figure 7 Manganese intrinsic lattice parameters.

of BGO and BTO lattices (Figure 6) reveal an obvious compatibility with the cubic main metric and angular parameters of the Mn intrinsic lattice.

Consecutively, a thorough study of BSO structures revealed a strong incompatibility with the Mn cubic lattice in terms of both bond lengths and angles (Figure 7).

Finally, a possible explanation for the paradox of disparity of incorporation behaviors of doping agent is formulated as follows: 'The stability of doping agents inside host structures is favored through geometrical compatibility, expressed in terms of matching patterns between doping agent intrinsic lattice and those of the host'.

Of course, it is the matter of a necessary but not sufficient condition. Nevertheless, many elements of this theory are already in good agreement with the results obtained by Van der Merwe,²⁵ Ischimura *et al.*²⁶ and Tuilier *et al.*²⁷

References

- 1 A. Duk, J. Schwarzkopf, A. Kwasniewski, M. Schmidbauer and R. Fornari, *Mater. Res. Bull.*, 2012, **47**, 2056.
- 2 T. Chen, T. Zhang, J. Zhou, J. Zhang, Y. Liu and G. Wang, *Mater. Res. Bull.*, 2012, **47**, 1104.
- 3 N. F. Mott, *Nobel Prize Lecture*, 1977.
- 4 W. W. Li, J. J. Zhu, J. D. Wu, J. Sun, M. Zhu, Z. G. Hu and J. H. Chu, *ACS Appl. Mater. Interfaces*, 2010, **2**, 2325.
- 5 H. Kimura, T. Fukumura, M. Kawasaki, K. Inaba, T. Hasegawa and H. Koinuma, *Appl. Phys. Lett.*, 2002, **80**, 94.
- 6 S. J. Liu, C. Y. Liu, J. Y. Juang and H. W. Fang, *J. Appl. Phys.*, 2009, **105**, 013928.
- 7 B. Liu, C. W. Cheng, R. Chen, Z. X. Shen, H. J. Fan and H. D. Sun, *J. Phys. Chem. C*, 2010, **114**, 3407.

- 8 G. Sanon, R. Rup and A. Mansingh, *Phys. Rev. B*, 1991, **44**, 5672.
- 9 L. F. Jiang, W. Z. Shen and Q. X. Guo, *J. Appl. Phys.*, 2009, **106**, 013515.
- 10 D. Davazoglou, *Appl. Phys. Lett.*, 1997, **70**, 246.
- 11 F. M. Pontes, E. Longo, J. H. Rangel, M. L. Bernardi, E. R. Leite and J. A. Varela, *Mater. Lett.*, 2000, **43**, 249.
- 12 Y. A. Borovlev, N. V. Ivannikova, V. N. Shlegel, Y. V. Vasiliev and V. A. Gusev, *J. Cryst. Growth*, 2001, **229**, 305.
- 13 *Topics in Applied Physics*, vol. 61, *Photorefractive Materials and Their Applications: Fundamental Phenomena*, eds. P. Günter and J.-P. Huignard, Springer-Verlag, Berlin, 1988.
- 14 H. J. Tiziani, *Opt. Acta*, 1982, **29**, 463.
- 15 W. Wardzynski, H. Szymczak, K. Pataj, T. Kasiwicz and J. Zmija, *J. Phys. Chem. Solids*, 1982, **43**, 767.
- 16 H. Chen, W. Zhu, E. Kaxiras and Z. Zhang, *Phys. Rev. B*, 2009, **79**, 235202.
- 17 F. Meng, R. Cui and W. Z. Shen, *J. Appl. Phys.*, 2001, **90**, 3387.
- 18 A. Iribarren, R. Castro-Rodriguez, V. Sosa and J. L. Pena, *Phys. Rev. B*, 1999, **60**, 4758.
- 19 *Handbook of Chemistry and Physics*, 35th edn., ed. C. D. Hodgman, Chemical Rubber Publishing Co., Cleveland, 1953, vol. 2, p. 2737.
- 20 *Handbook of Optics*, 2nd edn., ed. M. Bass, McGraw-Hill, Inc., New York, 1995, vol. 2, pp. 36–45.
- 21 P. Petkova and K. Boubaker, *J. Alloys Compd.*, 2013, **546**, 1769.
- 22 K. Boubaker, *ISRN Nanomaterials*, 2012, 4.
- 23 K. Boubaker, *J. Ceramics*, 2013, 6.
- 24 K. Boubaker, M. Amlouk, Y. Louartassi and H. Labiadh, *J. Aust. Ceram. Soc.*, 2013, **49**, 115.
- 25 J. H. Van der Merwe, *J. Electron. Mater.*, 1991, **20**, 793.
- 26 M. Ichimura and J. Narayan, *Philos. Mag. A*, 1995, **72**, 281.
- 27 M. H. Tuilier, H. Dexpert, P. Lagarde, M. Devalette and N. Khachani, *J. Phys. Chem. Solids*, 1987, **48**, 707.

Received: 22nd January 2013; Com. 13/4051